Quantum limit of the triplet proximity effect in half-metal–superconductor junctions

B. Béri,[1] J. N. Kupferschmidt,[2] C. W. J. Beenakker,[1] and P. W. Brouwer[2]
[1]*Instituut-Lorentz, Universiteit Leiden, P.O. Box 9506, 2300 RA Leiden, The Netherlands*
[2]*Laboratory of Atomic and Solid State Physics, Cornell University, Ithaca, New York 14853-2501, USA*
(Received 4 November 2008; published 26 January 2009)

We apply the scattering matrix approach to the triplet proximity effect in superconductor–half-metal structures. We find that for junctions that do not mix different orbital modes, the zero-bias Andreev conductance vanishes, while the zero-bias Josephson current is nonzero. We illustrate this finding on a ballistic half-metal–superconductor (HS) and superconductor–half-metal–superconductor (SHS) junctions with translation invariance along the interfaces and on HS and SHS systems where transport through the half-metallic region takes place through a single conducting channel. Our calculations for these physically single-mode setups—single-mode point contacts and chaotic quantum dots with single-mode contacts—illustrate the main strength of the scattering matrix approach. It allows for studying systems in the quantum mechanical limit, which is inaccessible for the quasiclassical Green's function methods, the main theoretical tool in previous works on the triplet proximity effect.

DOI: 10.1103/PhysRevB.79.024517 PACS number(s): 74.45.+c, 74.50.+r, 74.78.Na

I. INTRODUCTION

The recent experimental observation of the Josephson effect in a half-metallic junction between two superconducting reservoirs[1] has renewed interest in superconductor (S)-ferromagnet hybrid devices. The observation of a supercurrent in a half-metal (H) is remarkable because Cooper pairs in spin-singlet superconductors consist of a pair of electrons with opposite spin, whereas a half-metal conducts electrons of one spin direction only.[2–4] The resolution of this apparent paradox is the so-called "triplet proximity effect," which was first predicted theoretically by Bergeret *et al.*[5] (See also Refs. 6–8 as well as Ref. 9 for a review.) The triplet proximity effect relies on the conversion of spin-singlet Cooper pairs of electrons with opposite spin into pairs of electrons of equal spin at a spin-active interface between the superconductor and the half-metal.[5,6,8] Since pairs of equal-spin electrons can be transmitted coherently through a half-metal, the triplet proximity effect can indeed explain the observation of a Josephson current in the experiment.

Most theoretical studies of the triplet proximity effect were done using the quasiclassical Green's function method.[5–8,10–15] This method is appropriate for systems in which transport takes place through many conducting channels.[16,17] For systems with few channels only, the Green's function technique should be applied without the quasiclassical approximation. This, albeit doable,[12,13,15] can lead to calculations of significant complexity. Another method that is particularly well suited for few channel structures is the scattering matrix approach. This method has been frequently used in the context of transport problems involving superconductors (for a review, see Ref. 18). However, it has not yet been applied to the triplet proximity effect. It is the goal of the present paper to fill this gap.

In the language of the scattering approach, the triplet proximity effect relies on the coherent Andreev reflection of electronlike excitations into holelike excitations with the same spin.[19] Conventional Andreev reflection, as it takes place at the interface between a normal metal and a superconductor, consists of the reflection of an electron into a hole with opposite spin. "Same spin" and "opposite spin" here refer to the spin band from which the electron and hole are taken. Since electron and hole from the same spin band have opposite angular momentum, conservation of angular momentum implies that electron and hole are from opposite spin bands. Hence, Andreev reflection of electrons into holes from the same spin band requires that the interface between the half-metal and the superconductor is spin active. Examples of appropriate spin-active interfaces are a thin ferromagnetic or half-metallic layer with a polarization that is noncollinear with the half-metal's polarization or a normal-metal spacer layer with strong spin-orbit scattering.

Our focus is on systems with the fewest number of channels possible, a single conducting channel at the Fermi level. This limit can be achieved by having single-channel contacts between the superconductor(s) and the half-metal. As an example of this limit, we use the scattering theory to address the simplest single-channel half-metal–superconductor (HS) junction that can display triplet proximity effect: a single-channel ferromagnetic or half-metallic ballistic point contact between H and S electrodes. To study a more complex situation, we investigate HS and superconductor–half-metal–superconductor (SHS) junctions where the half-metal is a chaotic quantum dot with single-channel point contacts. We also study the case of ballistic devices which have translation invariance along the interfaces. This situation allows for a single-channel description as well since the translation symmetry ensures that different transverse modes do not mix. While the latter system can in principle be addressed by the quasiclassical Green's function method, the former physically single-channel setups are fully quantum mechanical, hence falling outside the scope of quasiclassics.

We use the scattering matrix approach to calculate the differential conductance of an HS junction and the (zero-bias) supercurrent in an SHS junction. We find that there is a remarkable difference between these two observables in the single-channel limit. For a single-channel half-metal–superconductor junction at zero temperature, the linear conductance vanishes at the Fermi level. The conductance be-

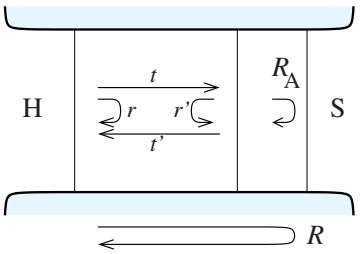

FIG. 1. (Color online) Composite HS junction consisting of a half-metallic contact (left), a superconducting contact (right), and a spin-active intermediate layer (center). In most of our considerations, the intermediate layer is taken to be ferromagnetic with a magnetization direction not collinear with the polarization of the half-metal. Transport through the HS junction is described by the scattering matrix $\mathcal{R}$, which is calculated in terms of the Andreev reflection matrix $\mathcal{R}_A$ of an ideal normal-metal–superconductor interface and the reflection and transmission matrices r, r', t, and t' of the nonsuperconducting region.

comes appreciable only if the applied voltage is comparable to the superconducting gap Δ or to the Thouless energy of the junction, whichever is smaller. The Josephson current, on the other hand, proves to be nonzero at zero temperature. The origin of this different behavior is that the Josephson effect contains information about the entire excitation spectrum of an SHS junction, whereas the linear conductance is a property that requires knowledge of excitations at the Fermi level only.

The remainder of this paper is organized as follows. In Sec. II we outline the key elements of the scattering approach and its application to HS junctions with a spin-active superconductor interface. In Secs. III and IV we then apply the scattering theory to transport through an HS junction and to the Josephson effect in an SHS junction, respectively. We conclude in Sec. V.

II. SCATTERING APPROACH

For a scattering description of the triplet proximity effect, we consider HS junctions that consist of a half-metal "end," a spin-active intermediate layer, and a superconductor. The intermediate layer may be half-metallic, ferromagnetic, or normal metallic.

The central object in the scattering approach is the scattering matrix $\mathcal{R}(\varepsilon)$ of the HS junction. It relates the amplitudes of excitations at energy $\varepsilon > 0$ propagating toward the superconductor and excitations propagating away from the superconductor at the half-metal end of the junction (see Fig. 1). If ε is below the superconducting gap Δ, all excitations must be reflected at the interface with the superconductor. This reflection can be of normal type (electronlike excitations are reflected as electrons and holelike excitations are reflected as holes) or of Andreev type (electronlike excitations are reflected as holes and vice versa). Both reflection types are contained in the matrix $\mathcal{R}$, which is made explicit by the decomposition

$$\mathcal{R}(\varepsilon) = \begin{pmatrix} r_{ee}(\varepsilon) & r_{eh}(\varepsilon) \\ r_{he}(\varepsilon) & r_{hh}(\varepsilon) \end{pmatrix}, \tag{1}$$

where r_{ee} and r_{hh} are matrices that describe normal reflection, whereas r_{eh} and r_{he} describe Andreev reflection. All four matrices have dimension N, the number of propagating modes at the Fermi level in H. Note that the propagating modes in H are not spin degenerate. Below, we will use the polarization direction of H as the spin quantization axis and refer to the electrons with spin parallel to the polarization direction of H as "spin up."

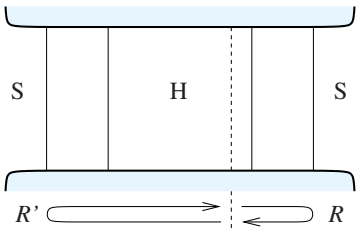

FIG. 2. (Color online) Schematic drawing of an SHS junction. In the scattering approach, an SHS junction is seen as two opposing (composite) HS junctions, with scattering matrices $\mathcal{R}'$ and $\mathcal{R}$, respectively. In the calculations of Sec. IV A, scattering phase shifts from the central half-metallic part are included into $\mathcal{R}'$.

Knowledge of the scattering matrix $\mathcal{R}$ is sufficient to calculate the conductance of an HS junction as well as the Josephson current in an SHS junction. The zero-temperature differential conductance of an HS junction reads[20,21]

$$G(eV) = \frac{2e^2}{h} \mathrm{Tr}\, r_{he}^{\dagger}(eV) r_{he}(eV). \tag{2}$$

(The factor of 2 accounts for the doubling of the current by the conversion of an electron into a hole.) An SHS junction can be viewed as two HS junctions opposed to each other (see Fig. 2). Denoting the scattering matrix corresponding to the second junction as $\mathcal{R}'$, the Josephson current reads[22]

$$I = -\frac{2ek_BT}{\hbar} \frac{d}{d\delta\phi} \sum_{n=0}^{\infty} \ln \det[1 - \mathcal{R}'(i\omega_n)\mathcal{R}(i\omega_n)], \tag{3}$$

where $\omega_n = (2n+1)\pi k_B T$ are the Matsubara frequencies and $\delta\phi$ is the phase difference between the two superconductors.

In principle, the explicit calculation of $\mathcal{R}$ requires a solution of the Bogoliubov-de Gennes equation for the full HS junction. Here, we take a different approach[23] and express $\mathcal{R}$ in terms of the scattering matrix $\mathcal{S}$ of the nonsuperconducting region—that is, the intermediate layer and the half-metallic region combined—and the reflection matrix $\mathcal{R}_A$ for Andreev reflection off an ideal normal-metal–superconductor interface. Using the same block structure as in Eq. (1), it reads

$$\mathcal{R}_A = \alpha(\varepsilon) \begin{pmatrix} 0 & i\sigma_2 e^{i\phi} \mathbb{1}_{N_S} \\ -i\sigma_2 e^{-i\phi} \mathbb{1}_{N_S} & 0 \end{pmatrix}, \tag{4}$$

where N_S is the number of propagating spin-degenerate orbital modes at the Fermi level at the superconductor interface, σ_2 is the Pauli matrix acting in spin space, ϕ is the phase of the superconducting order parameter, and

$$\alpha(\varepsilon) = e^{-i \arccos(\varepsilon/\Delta)}. \tag{5}$$

The scattering matrix $\mathcal{S}$ has the structure

$$\mathcal{S} = \begin{pmatrix} S(\varepsilon) & 0 \\ 0 & S(-\varepsilon)^* \end{pmatrix}, \tag{6}$$

where $S(\varepsilon)$ is the scattering matrix describing the scattering of electronlike excitations off the nonsuperconducting region. The scattering matrix $S(\varepsilon)$ can be further divided into transmission and reflection blocks,

$$S = \begin{pmatrix} r & t' \\ t & r' \end{pmatrix}, \tag{7}$$

where r describes reflection for electrons coming from H, r' describes reflection for electrons coming from the superconductor interface, and t and t' describe transmission from and to H. The matrices r and r' have dimension N and $2N_S$, respectively. Solving for the total scattering matrix $\mathcal{R}$ in terms of $\mathcal{R}_A$ and $\mathcal{S}$, one then finds

$$r_{ee} = r + \alpha^2 t' \sigma_2 r'^* \sigma_2 (1 - \alpha^2 r' \sigma_2 r'^* \sigma_2)^{-1} t, \tag{8a}$$

$$r_{eh} = ie^{i\phi} \alpha t' \sigma_2 (1 - \alpha^2 r'^* \sigma_2 r' \sigma_2)^{-1} t^*, \tag{8b}$$

$$r_{he} = -ie^{-i\phi} \alpha t'^* \sigma_2 (1 - \alpha^2 r' \sigma_2 r'^* \sigma_2)^{-1} t, \tag{8c}$$

$$r_{hh} = r^* + \alpha^2 t'^* \sigma_2 r' \sigma_2 (1 - \alpha^2 r'^* \sigma_2 r' \sigma_2)^{-1} t^*. \tag{8d}$$

Here we suppressed the energy arguments; the complex conjugate matrices in Eq. (7) should be taken at energy $-\varepsilon$.

In the scattering matrix approach, a necessary condition for the superconducting proximity effect is to have a nonvanishing r_{he}. For an HS junction, having a nonzero r_{he} is not automatic. In the absence of spin-flip scattering in the intermediate layer, an electron coming from H is Andreev reflected as a spin-down hole. This cannot re-enter the half-metallic contact; it is reflected from the half-metal instead, upon which it is Andreev reflected once more to return as a spin-up electron. Andreev reflection can occur only if the intermediate layer is spin active; that is, its scattering matrix is *not* diagonal in the spin up/down basis of the half-metallic contact. Such anomalous Andreev reflection, in which a spin-up electron coming from the half-metallic contact is reflected as a spin-up hole, is the key to the triplet proximity effect. Examples of spin-active layers that make this possible are a ferromagnet with a magnetization direction not collinear with the polarization of the half-metal, a normal metal with strong spin-orbit coupling, or a half-metallic spacer layer with a different polarization direction and thin enough that there is nonzero transmission of minority electrons through evanescent modes. In Secs. III and IV we use the scattering theory to calculate the conductance of an HS junction and the Josephson current in an SHS junction.

III. HS JUNCTIONS

A. General considerations

The scattering matrix $\mathcal{R}(\varepsilon)$ obeys particle-hole symmetry,

$$\mathcal{R}(\varepsilon) = \Sigma_1 \mathcal{R}(-\varepsilon)^* \Sigma_1, \tag{9}$$

where Σ_1 is the first Pauli matrix acting in electron-hole space. For the special case $N=1$, this symmetry, in combination with the condition that $\mathcal{R}(\varepsilon)$ is unitary, leads to the condition that either $r_{ee}=0$ or $r_{eh}=0$ at the Fermi level $\varepsilon=0$. As we show in the Appendix, generically one has $r_{eh}(0)=0$, although the possibility $r_{ee}(0)=0$ does occur for certain special choices of the spacer layer. The case $N=1$ is relevant for the case that the contact to the half-metal has only one propagating mode at the Fermi level or, alternatively, for the case that there is perfect translation symmetry in the transverse direction, so that different orbital modes do not mix. To the best of our knowledge, the observation that Andreev reflection at the Fermi level is absent for single-mode HS junctions has not been made before. It presents a qualitative difference compared to FS junctions in which both spin directions can propagate.

In the general theory of Sec. II the spin quantization axis is taken to be the polarization direction of the half-metal. Fixing the spin polarization axis still allows for rotations around that axis. For the scattering matrices appearing in the theory, such a rotation is represented by the transformation

$$S \to \begin{pmatrix} e^{i\psi/2} & 0 \\ 0 & e^{i\psi\sigma_3/2} \end{pmatrix} S \begin{pmatrix} e^{-i\psi/2} & 0 \\ 0 & e^{-i\psi\sigma_3/2} \end{pmatrix}, \tag{10}$$

where S is the scattering matrix of the nonsuperconducting region [see Eq. (6)], the block structure is that of Eq. (7), and ψ is the (azimuthal) angle of the rotation. Substituting this transformation into expression (8) for $\mathcal{R}$, one concludes that such a rotation has the same effect on $\mathcal{R}$ as a change in the superconducting order parameter ϕ as

$$\phi \to \phi + \psi. \tag{11}$$

A consequence of this observation is that, if the intermediate layer is ferromagnetic or half-metallic with a polarization along the unit vector

$$\mathbf{m} = (\sin\theta\cos\psi, \sin\theta\sin\psi, \cos\theta)^T, \tag{12}$$

which makes an angle θ with the polarization direction of the half-metallic contact, $\mathcal{R}$ is a function of the difference $\phi - \psi$ only. (Here, and in what follows, the polarization of the half-metal is taken to be along the z axis.) This observation, which will be important in our discussion of the Josephson effect in SHS junctions below, was first made by Braude and Nazarov[10] using the quasiclassical approach. Here, it appears as a natural consequence of the transformation rules of the scattering matrix under rotations.

B. Ballistic HS junction with ferromagnetic spacer

As a first and simplest application of the theory, we consider an HS junction for which the intermediate layer is a ferromagnet. The ferromagnet's magnetization points along the unit vector given in Eq. (12). We take the interfaces on both sides of the ferromagnetic spacer layer F to be ideal and assume that the electron motion in F is ballistic. In that case, different orbital modes decouple, and one can use an effective single-mode description for each orbital mode μ separately. We also assume that the thickness of F is short in comparison to the superconducting coherence length $\xi_S = \hbar v_F/\Delta$ (v_F is the Fermi velocity), so that the energy depen-

dence of the scattering matrix S can be neglected, and we assume that the magnetic flux through F is small in comparison to the flux quantum, so that the orbital motion is time-reversal symmetric.

For this system, the calculation of S requires the composition of the 4×4 scattering matrix of the ballistic ferromagnetic spacer layer,

$$S_F = \begin{pmatrix} 0 & U \\ U & 0 \end{pmatrix}, \quad U = e^{i(\eta+\rho\mathbf{m}\cdot\boldsymbol{\sigma})/2}, \tag{13}$$

and the 3×3 scattering matrix S_H of the ideal interface between the half-metallic contact and the ferromagnetic spacer layer,

$$S_H = \begin{pmatrix} 0 & 1 & 0 \\ 1 & 0 & 0 \\ 0 & 0 & e^{i\beta} \end{pmatrix}. \tag{14}$$

In the above expressions, $\boldsymbol{\sigma}$ is the vector of Pauli matrices (acting in spin space), $\rho=\nu_\uparrow-\nu_\downarrow$ is the difference of the phase shifts of majority and minority electrons in F upon propagation through the spacer layer, and $\eta=\nu_\uparrow+\nu_\downarrow$. In Eq. (14), β is the phase-shift spin-down electrons experience upon reflection from the half-metallic contact. The three phases ρ, η, and β depend on the orbital mode μ. We have suppressed the mode dependence here but will restore it in the final expression [Eq. (16) below]. The block structure of S_F is as in Eq. (7). The same is true for S_H, where the lower right 2×2 submatrix corresponds to the lower right block in Eq. (7).

Combining Eqs. (13) and (14) to calculate S, and then using Eq. (8) to find $\mathcal{R}$, we obtain

$$\mathcal{R}(\varepsilon) = \frac{\alpha^2}{1+\alpha^2\sin^2\rho\sin^2\theta}\begin{pmatrix} e^{-i\beta}(\cos\rho + i\sin\rho\cos\theta)^2 & -2i(\varepsilon/\Delta)e^{i(\phi-\psi)}\sin\theta\sin\rho \\ -2i(\varepsilon/\Delta)e^{i(\psi-\phi)}\sin\theta\sin\rho & e^{i\beta}(\cos\rho - i\sin\rho\cos\theta)^2 \end{pmatrix}. \tag{15}$$

Substituting Eq. (5) for α and summing over all orbital modes μ, we conclude that the differential conductance of a short ballistic HFS junction is

$$G(\varepsilon) = \sum_\mu \frac{8e^2}{h} \times \frac{\varepsilon^2\sin^2\theta\sin^2\rho_\mu}{\Delta^2(1-\sin^2\theta\sin^2\rho_\mu)^2+4\varepsilon^2\sin^2\theta\sin^2\rho_\mu}, \tag{16}$$

where the summation is over the orbital modes in the HS junction.

This simple result illustrates the two main properties of the triplet proximity effect in HS junctions: first, Andreev reflection is possible as soon as there is a spacer layer that breaks spin-rotation symmetry around the half-metal's polarization direction provided that the electron's spin precesses by an angle different from 0 or π. [In Eq. (16) this translates to the requirement that $\sin\theta\neq0$ and $\sin\rho_\mu\neq0$.]; and second, in the absence of orbital mode mixing, $G=0$ at the Fermi level, except for very special choices of the thickness (proportional to ρ_μ) and magnetization direction of the spacer layer. In the present case, these special choices are angles θ and ρ_μ for which $\sin^2\theta=\sin^2\rho_\mu=1$. In that case, one finds $G=(2e^2/h)M$, where M is the number of modes with $\sin^2\rho_\mu=1$.

Unlike the quasiclassical approach, the scattering approach can also deal with systems in which the number of orbital modes is small. The simplest way to illustrate this is to consider the contribution of one orbital mode; in this case, the result in Eq. (15) and the corresponding term in Eq. (16) describe a single-mode ballistic ferromagnetic quantum point contact between the half-metal and the superconductor. In Fig. 3 we show the differential conductance of such an HS quantum point contact for a few representative values of the ferromagnet parameters ρ and θ. Both aforementioned features are clearly seen. The conductance decreases as $\sin^2\theta$ and $\sin^2\rho$ decreases, and it vanishes at the Fermi energy.

C. Ballistic HS junction with half-metallic spacer

If the spacer layer between the half-metallic reservoir and the superconductor is not a ferromagnet, but a half-metal, transmission through the minority channel is via evanescent modes, not propagating waves. The scattering matrix of the spacer layer, which was given by Eq. (13) for the case of a ferromagnetic spacer, now reads

$$S_{H'} = e^{-i\sigma_z\psi/2}e^{-i\sigma_y\theta/2}S'e^{i\sigma_y\theta/2}e^{i\sigma_z\psi/2}, \tag{17}$$

where

$$S'_{H'} = \begin{pmatrix} 0 & 0 & e^{i\nu_\uparrow} & 0 \\ 0 & -ie^{i\nu_\downarrow}\sqrt{1-\tau} & 0 & e^{i\nu_\downarrow}\sqrt{\tau} \\ e^{i\nu_\uparrow} & 0 & 0 & 0 \\ 0 & e^{i\nu_\downarrow}\sqrt{\tau} & 0 & -ie^{i\nu_\downarrow}\sqrt{1-\tau} \end{pmatrix}. \tag{18}$$

The (mode-dependent) phase shift $\nu_\downarrow$ and transmission coefficient τ for minority electrons are functions of the wave function decay rate q and effective mass $m_\downarrow$ of the evanescent minority electron wave functions, the velocity v of the majority electrons, and the thickness d of the half-metallic spacer layer. If $qd\gg1$, the minority electron phase shift $\nu_\downarrow$

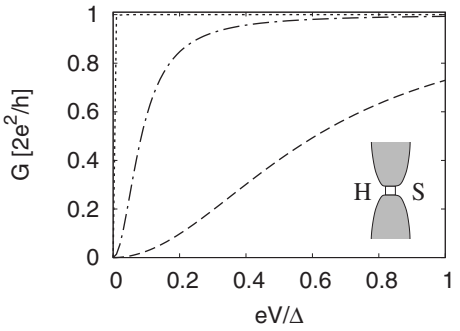

FIG. 3. The subgap differential conductance G versus the applied voltage V for a ballistic single-mode HS quantum point contact. The small gray rectangle in the contact represents a region with a different magnetization than in the half-metallic part. Physically such a region can be present due to a misaligned magnetization at the half-metal surface (Ref. 14). In our calculations this corresponds to the ferromagnetic spacer layer. The curves correspond to different values of the phase angles in the ferromagnetic spacer, $\theta=0.8$ and $\rho=0.9$ (dashed curve), $\theta=1.4$ and $\rho=1.2$ (dashed-dotted curve), and $\theta=1.56$ and $\rho=1.53$ (dotted curve).

becomes independent of the layer thickness d,

$$-ie^{i\nu_\downarrow}=e^{i\beta}=\frac{v-i\hbar q/m_\downarrow}{v+i\hbar q/m_\downarrow}, \tag{19}$$

whereas the transmission coefficient $\tau\propto e^{-2qd}$ and $\nu_\uparrow=m_\uparrow vd/\hbar$, where $m_\uparrow$ is the effective mass of majority electrons. [The phase shift β is the reflection phase for minority electron reflection off a half-infinite half-metal; see Eq. (14) above.]

With the definitions $\rho=\nu_\uparrow-\nu_\downarrow$ and $\eta=\nu_\uparrow+\nu_\downarrow$, we then find that the conductance of an HS junction with a half-metallic spacer is

$$G=\frac{8e^2}{h}\sum_\mu \frac{\varepsilon^2\Delta^2\tau_\mu[\sin\rho_\mu+(1-\tau_\mu)^{1/2}\sin\eta_\mu]^2\sin^2\theta}{(B_0\Delta^2-B_1\varepsilon^2)^2+4B_2^2\varepsilon^2(\Delta^2-\varepsilon^2)}, \tag{20}$$

where we abbreviated

$$B_0=[\sin\rho_\mu\cos\theta+(1-\tau_\mu)^{1/2}\sin\eta_\mu]^2+[\cos\rho_\mu+(1-\tau_\mu)^{1/2}\cos\eta_\mu]^2,$$

$$B_1=2+(1+\cos^2\theta)(1-\tau_\mu)+2(1-\tau_\mu)^{1/2}\cos(\eta_\mu-\rho_\mu)(1+\cos\theta),$$

$$B_2=1+(1-\tau_\mu)^{1/2}\cos(\eta_\mu-\rho_\mu)(1+\cos\theta)+(1-\tau_\mu)\cos\theta,$$

and restored the summation over the orbital modes μ. For τ_μ close to unity, this expression simplifies to the Andreev conductance for an HS junction with a ferromagnetic spacer [Eq. (16) above]. For small energies one may neglect the terms proportional to ε^2 and ε^4 in the denominator, and we find that $G\propto\varepsilon^2\tau$. Since the transmission coefficients τ_μ are exponentially small if $q_\mu d\gg 1$, the conductance is dominated by the transverse mode μ with the lowest q_μ.

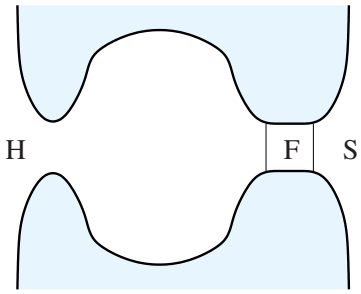

FIG. 4. (Color online) Chaotic HS junction, consisting of a half-metallic contact (left), a half-metallic quantum dot (center), a ferromagnetic spacer layer, and a superconducting contact (right).

Similar to the case of ideal transmission, there is a special set of parameters at which the conductance becomes large, independent of transmission. This occurs when the coefficient $B_0=0$ in Eq. (20), so that the denominator in that equation vanishes at $\varepsilon=0$. The condition $B_0=0$ translates to

$$\cos\rho_\mu=-(1-\tau_\mu)^{1/2}\cos\eta_\mu,$$

$$\sin\rho_\mu\cos\theta=-(1-\tau_\mu)^{1/2}\sin\eta_\mu. \tag{21}$$

Solutions of Eq. (21) satisfy the relation $\sin^2\rho_\mu\sin^2\theta=\tau_\mu$, which generalizes the condition for resonance found for a ferromagnetic spacer layer (corresponding to $\tau_\mu=1$). Since $\nu_{\downarrow\mu}=(\eta_\mu-\rho_\mu)/2$ is a material property if $q_\mu d\gg 1$ [see Eq. (19) above], ρ_μ and η_μ are not independent in that limit. For a specific half-metallic material and in the limiting case $q_\mu d\gg 1$, the relevant solution of Eq. (21) then becomes $(\rho_\mu+\eta_\mu)/2=\nu_{\uparrow\mu}=\pi/2 \bmod \pi$ and $\theta\to\pi$. Since $\nu_{\uparrow\mu}$ is a function of the thickness d of the spacer layer, not a material property, this condition can always be satisfied for special values of d. If a mode satisfies conditions (21), its contribution to the conductance is

$$G_{\mathrm{res},\mu}=\frac{2e^2}{\hbar}\frac{4\Delta^2\tau_\mu^2}{4\Delta^2\tau_\mu^2+\varepsilon^2\{[1-\cos\theta+\tau_\mu(1+\cos\theta)]^2-4\tau_\mu^2\}}. \tag{22}$$

At zero energy, one finds perfect Andreev reflection irrespective of τ_μ. As before, the contribution of a single orbital mode in Eqs. (20) and (22) describes the differential conductance of a single-mode quantum point contact with a misaligned half-metallic surface layer at the constriction. The analog of the setup is sketched in Fig. 3.

D. Chaotic HS junction

As the next application of the scattering method, we consider a "chaotic HS junction," which consists of a half-metallic contact, a chaotic quantum dot, a ferromagnetic contact, and a superconductor all connected in series (see Fig. 4). To illustrate the strengths of the scattering matrix approach, we focus on a situation that is intractable with quasiclassical methods. We restrict our discussion to the case that both contacts have one orbital mode only.

For definiteness, we take the quantum dot to be half-metallic, with the same polarization direction as the half-

metallic contact. Two alternative scenarios, a normal-metal quantum dot and a ferromagnetic quantum dot with a magnetization direction parallel to that of the half-metallic contact, will be addressed at the end of this section. In all cases we assume that the typical electron path length before exiting from the dot through one of the contacts is short compared to the superconducting coherence length.

The calculation proceeds similar to that of the ballistic junction shown above. For the chaotic HS junction with a half-metallic quantum dot, we replace the scattering matrix S_H of Eq. (14) by

$$S_H = \begin{pmatrix} -e^{i\chi}\sqrt{1-\tau} & e^{i(\chi+\xi)/2}\sqrt{\tau} & 0 \\ e^{i(\chi+\xi)/2}\sqrt{\tau} & e^{i\xi}\sqrt{1-\tau} & 0 \\ 0 & 0 & e^{i\beta} \end{pmatrix}, \tag{23}$$

where $0 \leq \tau \leq 1$ is the transmission coefficient of the quantum dot and ξ and χ are scattering phases for reflection off the quantum dot. As before, β is the phase-shift minority electrons acquire when they are reflected off the half-metal. The special case $\tau=1$ simplifies to the ballistic HS point contact we considered previously. For general τ, one finds

$$G(\varepsilon) = \frac{2e^2}{h}\frac{16\varepsilon^2\Delta^2\tau^2 \sin^2\rho \sin^2\theta}{D(\varepsilon)}, \tag{24}$$

where

$$D = \{\Delta^2(1-\tau)^{1/2}[4\cos\theta\sin(\beta-\xi)\sin(2\rho) + \cos(\beta-\xi)[1-2\cos(2\theta)\sin^2\rho + 3\cos(2\rho)]] + 2(\tau-2) \times (2\varepsilon^2 + \Delta^2\sin^2\rho\sin^2\theta - \Delta^2)\}^2 + 16\varepsilon^2(\Delta^2-\varepsilon^2)\tau^2. \tag{25}$$

For the special point $\sin^2\theta = \sin^2\rho = 1$ one has $G(0) = 2e^2/h$, which is independent of τ and the scattering phases β, χ, and ξ. The origin of this remarkable result is that, for $\sin^2\theta = \sin^2\rho = 1$, the ferromagnet-superconductor interface not only provides perfect Andreev reflection between spin-up electrons and spin-up holes, but, moreover, after two subsequent Andreev reflections the net phase shift is $-\alpha^2 = 1$ at the Fermi energy. Hence, combining the interface reflection matrix (15) with the scattering matrix of the quantum dot, the conductance at vanishing voltage is found to be

$$\frac{h}{2e^2}G(0) = \tau^2/[1-(1-\tau)]^2 = 1, \tag{26}$$

which is independent of the dot's transmission coefficient τ. This is to be contrasted to the corresponding formula formula[23]

$$\frac{h}{2e^2}G(0) = \tau^2/[1+(1-\tau)]^2 \tag{27}$$

for the linear-response conductance (per spin) of a superconductor in contact with a single-mode quantum dot through a normal-metal contact (and without magnetic a field). The difference arises from the fact that, in the latter case, the phase shift upon two Andreev reflections is $\alpha^2 = -1$ at the Fermi energy.

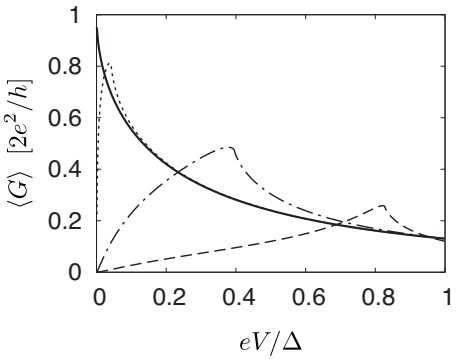

FIG. 5. The ensemble-averaged subgap differential conductance $\langle G\rangle$ versus the applied voltage V for different phase angles θ and ρ describing the ferromagnetic contact. The values of θ and ρ are 0.8 and 0.9 (dashed curve), 1.4 and 1.2 (dashed-dotted curve), and 1.56 and 1.53 (dotted curve), respectively. The solid curve shows the special case corresponding to $\theta = \rho = \pi/2$.

For a chaotic quantum dot, the transmission coefficient τ and the scattering phases $0 < \xi, \chi < 4\pi$ are random quantities with the statistical distribution[18]

$$P(\tau,\xi,\chi) = \frac{1}{32\pi^2}\tau^{-1/2}. \tag{28}$$

As is standard in the statistical approach to quantum transport, the statistical ensemble is obtained by means of small variations in the dot's shape or in the Fermi energy. In an experiment, both types of variations can be achieved by changing the voltage of nearby metal gates. With the help of the distribution (28) we can calculate the average Andreev conductance $\langle G\rangle$ for an ensemble of quantum dots. The phase shift ρ, the angle θ, and the reflection phase β are not averaged over since they are properties of the ferromagnetic contact and the half-metal interface, not of the chaotic quantum dot. The average can be performed analytically in the special case $\sin^2\rho = \sin^2\theta = 1$, for which we find

$$\langle G\rangle = \frac{2e^2}{h}\left(1 - \frac{\Delta^2}{4\varepsilon(\varepsilon^2-\Delta^2)^{1/2}}S\right) \tag{29}$$

with

$$S = \sum_{\pm} \pm x_{\pm}^3 \operatorname{artanh}\frac{1}{x_{\pm}}, \tag{30}$$

where

$$x_{\pm}^2 = \frac{2\varepsilon[\varepsilon \pm (\varepsilon^2-\Delta^2)^{1/2}]}{\Delta^2}. \tag{31}$$

At the Fermi level $\langle G\rangle = 2e^2/h$, in agreement with the discussion following Eq. (25). For general values of θ and ρ no closed-form expression for $\langle G\rangle$ could be obtained. The result of a numerical evaluation of the ensemble average $\langle G(\varepsilon)\rangle$ is shown in Fig. 5 for a few representative values of θ and ρ. For generic θ and ρ, the ensemble-averaged conductance vanishes at the Fermi level $\varepsilon = 0$. The quadratic dependence $G \sim \varepsilon^2$ for $\varepsilon \to 0$ changes to a linear increase for relatively small voltages. The conductance reaches a maximum at a

voltage eV below the superconducting gap Δ for θ,ρ sufficiently away from $\sin\theta=0,\sin\rho=0$. With θ,ρ approaching $\sin\theta=0,\sin\rho=0$, the position of the maximum moves toward the superconducting gap Δ. For θ,ρ close to $\sin\theta=0,\sin\rho=0$, the conductance is an increasing function of the voltage in the full subgap regime.

For the case of a normal-metal quantum dot, the conductance $G(\varepsilon)$ is given by Eq. (24) but with the replacement $\beta-\xi\rightarrow\arctan\{\tau\sin(\beta+\chi)/[(2-\tau)\cos(\beta+\chi)+2(1-\tau)^{1/2}]\}$. For the case of a ferromagnetic quantum dot with a magnetization direction along that of the polarization of the half-metallic contact, $G(\varepsilon)$ is given by Eq. (24) but with $\beta-\xi$ replaced with a phase shift β' that is statistically independent of χ, ξ, and τ. In both cases, the qualitative dependence of $\langle G\rangle$ on the parameters ε, θ, and ρ is the same as in the case of a half-metallic quantum dot discussed above.

IV. SHS JUNCTIONS

We now contrast the transport current through an HS junction to the supercurrent through an SHS junction. As in Sec. III, we consider the effect of a thin ferromagnetic layer between each superconductor and the adjacent half-metal. (We do not consider the case of a thin half-metallic spacer layer in this section.) While, at zero temperature, the zero-bias conductance of a single single-channel HS junction vanishes (except at special choices of the parameters), the zero-temperature Josephson current I is not zero. The reason is that, in contrast to the linear-response conductance G, I is not a Fermi-level property. Instead, it is determined by the full excitation spectrum.

In order to apply the theory of Secs. I–III, we consider the SHS junction as two opposing HS junctions (see Fig. 2). We refer to the opposing HS junction as S′H. Both junctions have intermediate ferromagnetic layers, which are denoted by F and F′. The two ferromagnets can have different magnetizations parametrized by polar angles θ,ψ and θ',ψ', respectively. The superconductors S and S′ are assumed to have equal superconducting gaps Δ, but the phases ϕ and ϕ' of the order parameters can be differ.

Before turning to applications of our scattering theory, it is worthwhile to summarize some general considerations. Because of the transformation property (11), the Josephson current I can depend on the superconducting phases ϕ and ϕ' and on the azimuthal angles ψ and ψ' through the single combination

$$\tilde{\phi}=\phi-\phi'-(\psi-\psi') \tag{32}$$

only. This observation was made previously in the context of the quasiclassical approach.[10,11,14]

Under the operation of time reversal, the phases of the superconductors and the (position dependent) magnetization direction $\mathbf{m}$ transform as $\phi\rightarrow-\phi$ and $\mathbf{m}\rightarrow-\mathbf{m}$. The supercurrent of the time-reversed system is the opposite of the original, that is,

$$I(\phi-\phi',\mathbf{m})=-I(\phi'-\phi,-\mathbf{m}). \tag{33}$$

The supercurrent is invariant under a position-independent rotation of the magnetization. This, together with Eq. (33) results in $I(\tilde{\phi})=-I(-\tilde{\phi})$.

For phase angles not close to the special point $\sin^2\theta=\sin^2\theta'=\sin^2\rho=\sin^2\rho'=1$, the Andreev reflection probability at the SH interfaces is significantly smaller than unity [see Eq. (15) above]. As a consequence, the $\tilde{\phi}$ dependence of the supercurrent is nearly sinusoidal in this case. The detailed calculations of Sec. IV A and IV B show, however, that close to the special values of the phase angles the $\tilde{\phi}$ dependence becomes nonsinusoidal.

As an illustration of our scattering theory, we now consider the ballistic and chaotic junctions addressed in Sec. III. Our work on the Josephson effect in ballistic junctions complements that of Galaktionov *et al.*,[15] who used the Green's function approach.

A. Ballistic SHS junction

For the ballistic SHS junction different orbital modes are not mixed, so that the scattering problem is effectively one dimensional. As before, we denote the difference of the (mode-dependent) phase shifts of majority and minority electrons transmitted through F by ρ [see Eq. (13)]. The corresponding quantity for F′ is denoted by ρ'. We suppress the mode index μ except in the final expressions. For the calculation of the supercurrent, it is necessary that phase shifts accumulated inside the half-metal are included into the determinant in Eq. (3). For an orbital mode μ these phase shifts depend on the length L of the half-metallic segment and on the longitudinal component $k_\mu(\varepsilon)=k_\mu(0)+\varepsilon/(\hbar v_\mu)$ of the wave vector for that mode, where v_ν is the group velocity of the mode at $k_\mu(0)$. In order to include this into Eq. (3) we take the scattering matrix $\mathcal{R}'$ to include the scattering phase shifts accumulated inside the half-metal,

$$\mathcal{R}'=\begin{pmatrix} e^{ik_\mu(\varepsilon)L} & 0 \\ 0 & e^{-ik_\mu(-\varepsilon)L}\end{pmatrix}\tilde{\mathcal{R}}'\begin{pmatrix} e^{ik_\mu(\varepsilon)L} & 0 \\ 0 & e^{-ik_\mu(-\varepsilon)L}\end{pmatrix}, \tag{34}$$

where $\tilde{\mathcal{R}}'$ is the reflection matrix for the S′H junction without the scattering phases from the half-metal. This matrix is given in Eq. (15) of Sec. III but with θ, ψ, ϕ, and ρ replaced with θ', ψ', ϕ', and ρ', respectively.

Since there is a probability of normal reflection at each end of the SHS junction, for a given orbital mode, the contribution to the supercurrent contains terms that oscillate with the length L of the junction. For the total supercurrent obtained by summing the contributions from different orbital modes, however, this results only in a small correction, provided that $k_\mu(0)L\gg1$, since in this case, the sum of the oscillating contributions averages out. Below, we calculate the nonoscillating contribution to the Josephson current for a given orbital mode and restrict our discussion to the limiting cases of a "short junction" ($L\ll\xi_S$) and a "long junction" ($L\gg\xi_S$). (In both cases, we assume that the ferromagnetic spacer layers are thin in comparison to the superconducting

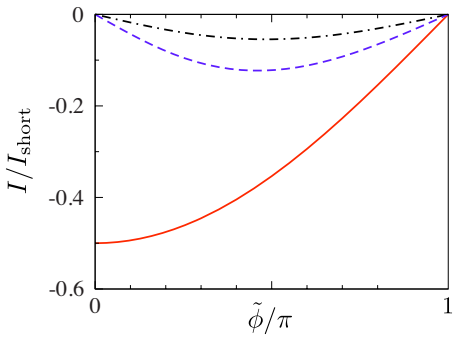

FIG. 6. (Color online) The contribution of a single transverse mode to the zero-temperature supercurrent I of a short SHS junction, as a function of $\tilde{\phi}$, for ferromagnetic phase angles $\theta=\theta'=\rho=\rho'=\pi/2$ (solid curve), $\theta=\theta'=\rho=\rho'=\pi/4$ (dotted-dashed curve), and $\theta=\theta'=\pi/2, \rho=\rho'=\pi/4$ (dashed curve). The supercurrent is shown in units of $I_{\rm short}=e\Delta/\hbar$.

coherence length ξ_S. The same assumption was made in Sec. III.)

For a short junction, one may neglect the energy dependence of the wave number $k_\mu(\varepsilon)$ in the half-metal. A closed-form expression valid for arbitrary temperatures could be obtained for the special case $\sin^2\theta=\sin^2\theta'=1$ for a mode μ with $\sin^2\rho_\mu=\sin^2\rho'_\mu=1$ only. The contribution I_μ to the supercurrent of such a mode is

$$I_\mu=-\frac{e\Delta}{2\hbar}\cos\frac{\tilde{\phi}+s_\mu\pi}{2}\tanh\left(\frac{\Delta}{2k_BT}\sin\frac{\tilde{\phi}+s_\mu\pi}{2}\right), \quad (35)$$

where s_μ is defined through the relation

$$(-1)^{s_\mu}=\sin\rho_\mu\sin\rho'_\mu. \quad (36)$$

The π shift in the current-phase relationship associated with s_μ originates from the properties of the interface reflection matrix (15). For this matrix, the transformation $\rho\to\rho+\pi$ is equivalent to $\phi\to\phi+\pi$.

In the limit of high temperatures $k_BT\gg\Delta$, one can find a closed-form expression for arbitrary values of θ, θ', ρ, and ρ'. Upon summation over all orbital modes, one has

$$I=-\sum_\mu\frac{e}{\hbar}\frac{\Delta^2}{8k_BT}\sin\tilde{\phi}\sin\rho_\mu\sin\rho'_\mu\sin\theta\sin\theta'. \quad (37)$$

Note that although the angles ρ_μ,ρ'_μ are mode dependent, for sufficiently thin spacer layers the mode dependence is weak enough that all modes contribute to the total Josephson current with the same sign. The supercurrent is reduced once the thickness of the spacer layers is large enough that $\rho_\mu,\rho'_\mu\gg1$.

A numerical evaluation of the contributions to the zero-temperature supercurrent is shown in Fig. 6 for a few choices of the angles θ, θ', ρ, and ρ'. Although the discontinuity at $\tilde{\phi}=s\pi$ is smeared for generic values of the phase angles, the order of magnitude of the supercurrent is the same as at the special point $\sin^2\theta=\sin^2\theta'=\sin^2\rho=\sin^2\rho'=1$. This is in contrast to the Fermi-level conductance of an HS junction, which was zero for generic phase angles and finite at the special point. As discussed above, the reason why the supercurrent has a different behavior is that it is not a Fermi-level property but, instead, depends on the entire excitation spectrum. For energies far away from the Fermi level, the Andreev conductance is not qualitatively different at the special point and elsewhere (see Fig. 3).

For a long SHS junction (but still with ferromagnetic spacer layers that are much thinner than ξ_S), again a compact expression at arbitrary temperatures could be obtained for the special case $\sin^2\theta=\sin^2\theta'=1$ for the contribution I_μ of a mode μ with $\sin^2\rho_\mu=\sin^2\rho'_\mu=1$ only. In this case one finds

$$I_\mu=-\frac{e}{\hbar}2k_BT\sum_n\frac{\sin(\tilde{\phi}+s_\mu\pi)}{\cosh(2\omega_nL/\hbar v_\mu)-\cos(\tilde{\phi}+s_\mu\pi)}, \quad (38)$$

where s_μ was defined in Eq. (36). At zero temperature the summation can be replaced with an integration and one has

$$I_\mu=\frac{ev_\mu[\tilde{\phi}-(1-s_\mu)\pi]}{2\pi L}, \quad 0<\tilde{\phi}+s_\mu\pi<2\pi. \quad (39)$$

In the limit of high temperatures, $T\gg\hbar v_\mu/L$, only the term with $n=0$ contributes, so that

$$I_\mu=-\frac{e}{\hbar}4k_BTe^{-2\pi k_BTL/\hbar v_\mu}\sin(\tilde{\phi}+s_\mu\pi). \quad (40)$$

The special point $\sin^2\theta=\sin^2\theta'=\sin^2\rho=\sin^2\rho'=1$ is singular, however, and the supercurrent contributions have a qualitatively different dependence on temperature for generic θ, θ', ρ, and ρ'. In the high-temperature regime $\hbar v_\mu/L\ll k_BT\ll\Delta$, one finds

$$I=-\frac{e}{\hbar}\frac{16\pi^2k_B^3T^3}{\Delta^2}\sum_\mu\sin\rho_\mu\sin\rho'_\mu\sin\theta\sin\theta'\sin\tilde{\phi}\times\frac{e^{-2\pi Lk_BT/\hbar v_\mu}}{(1-\sin^2\rho_\mu\sin^2\theta)(1-\sin^2\rho'_\mu\sin^2\theta')}. \quad (41)$$

This result is a factor of $\sim(k_BT/\Delta)^2\ll1$ smaller (per orbital mode) than the contribution for the special choice of the angles θ, θ', ρ, and ρ' in Eq. (40). Whereas the supercurrent of a short Josephson junction depends on the full subgap excitation spectrum of the junction,[24] the supercurrent in the long junction limit is determined by the junction's excitation spectrum up to the Thouless energy $\hbar v_F/L$ only.[22] In this range of the spectrum, the absence of Andreev reflection at the Fermi energy still strongly affects the magnitude of the supercurrent. For temperatures below the Thouless energy $\hbar v_F/L$ the suppression factor with which I_μ is reduced in comparison to the special case of Eq. (38) saturates around $(\hbar v_F/L\Delta)^2$. No closed-form expressions for I_μ at arbitrary temperatures could be obtained. Figure 7, shows I_μ versus $\tilde{\phi}$ at zero temperature, for two choices of the parameters θ, θ', ρ, and ρ'.

B. Chaotic SHS junction

For a chaotic SHS junction, we include the quantum dot into $\mathcal{R}$ and take $\mathcal{R}'=\tilde{\mathcal{R}}'$ to be the scattering matrix of a junction without quantum dot (see Fig. 8). For the chaotic

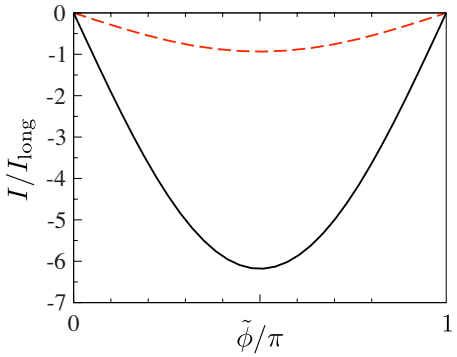

FIG. 7. (Color online) The contribution of a single transverse mode to the nonoscillating component of the zero-temperature supercurrent I of a long SHS junction, as a function of $\tilde{\phi}$, for ferromagnetic phase angles $\theta=\theta'=\rho=\rho'=\pi/3$ (solid curve) and $\theta=\theta'=\rho=\rho'=\pi/4$ (dashed curve). The current is shown in units of $I_{\rm long}=e\hbar^2 v_\mu^3/\pi L^3\Delta^2$, where v_μ is the mode-dependent longitudinal velocity.

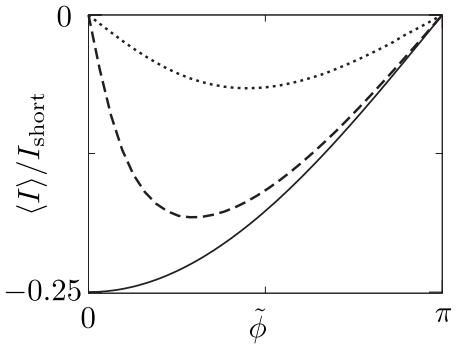

FIG. 9. The ensemble-averaged Josephson current $\langle I\rangle$ as a function of $\tilde{\phi}$ for different phase angles θ, ρ, θ', and ρ' describing the ferromagnetic spacer layers. The values of θ and ρ are $\theta=\rho=\pi/2$ (solid curve), $0.9(\pi/2)$ and $0.99(\pi/2)$ (dashed curve), and $0.5(\pi/2)$ and $0.6(\pi/2)$ (dotted curve), respectively. The values for the second contact are $\theta'=1.05(\pi/2)$ and $\rho'=0.95(\pi/2)$. The supercurrent is shown in units of $I_{\rm short}=e\Delta/\hbar$.

SHS junction we only consider the limit that the superconducting coherence length is much longer than the typical electron path length in the dot before exiting through one of the contacts.

In the special case $\sin^2\theta=\sin^2\theta'=\sin^2\rho=\sin^2\rho'=1$ the expression for the supercurrent is the same as for a ballistic SHS junction but with the replacement $\Delta\to\Delta\tau^{1/2}$, where τ is the transmission coefficient of the quantum dot. Since $\langle\tau^{1/2}\rangle=1/2$, at zero temperature, the ensemble-averaged supercurrent is

$$\langle I\rangle=-\frac{e\Delta}{4\hbar}\cos\frac{\tilde{\phi}+s\pi}{2},\quad 0<\tilde{\phi}+s\pi<2\pi, \tag{42}$$

where s was defined below Eq. (35). No closed-form expressions could be obtained for generic values of θ, θ', ρ, and ρ'. A numerical evaluation of the ensemble-averaged supercurrent is shown in Fig. 9. For phase angles close to the special case discussed above, the supercurrent in a short chaotic SHS junction follows Eq. (42) except near the discontinuity $\tilde{\phi}=s\pi$, which is smoothed out away from the special point $\sin^2\theta=\sin^2\theta'=\sin^2\rho=\sin^2\rho'=1$. For phase angles not close to the special point, the $\tilde{\phi}$ dependence of the ensemble-averaged supercurrent is nearly sinusoidal, confirming the general observations made in the beginning of this section.

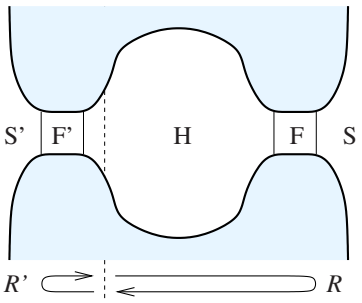

FIG. 8. (Color online) Superconductor–half-metal-quantum-dot–superconductor junction. In the calculation, scattering from the half-metal quantum dot is included in the scattering matrix $\mathcal{R}$.

V. CONCLUSION

For the conventional proximity effect, the possibility of Andreev reflection of electrons at the Fermi level gives a nonzero linear conductance through a normal-metal–superconductor interface. In this paper, we found that the situation is more delicate for the triplet proximity effect in half-metal–superconductor (HS) junctions. In the case that there is only one conducting channel at the HS interface, or that different orbital channels at the HS interface decouple, we found that Andreev reflection processes can be present only away from the Fermi level (except for special choices of the interface parameters). While this result, which is independent of the nature of the spin-active spacer layer in the HS junction, leads to a vanishing linear conductance, it allows for a nonzero Josephson current through an effectively single-channel SHS junction. We have illustrated this statement on systems both in the quasiclassical and in the fully quantum mechanical regimes. In our calculations we have mainly concentrated on the case of ferromagnetic spin-active intermediate layers.

First, we have calculated the zero-temperature differential Andreev conductance at finite bias for short HS junctions. This is the observable in which the present Andreev reflection processes manifest themselves in the most direct way. Using the scattering matrix approach, we calculated the dependence of the Andreev conductance on the phase angles of the spacer for all subgap voltages. Our result in Eq. (24) can be used to describe the conductance of a system with an arbitrary single-channel structure in the half-metal provided that its normal-state scattering matrix is known. As an application, we considered the case that the structure is a chaotic quantum dot and we calculated the ensemble-averaged conductance from the known distribution of the dot scattering matrices. In addition to the calculation of the differential conductance for systems with ferromagnetic spacer layer, we also studied ballistic systems where the spacer is a thin half-metallic layer.

Second, we calculated the zero-bias Josephson current through SHS junctions. We have confirmed the observation, reported in earlier works,[10,11,14] that the Josephson current depends on the superconducting phase through the single variable $\tilde{\phi}=\phi-\phi'-(\psi-\psi')$ only, which is the difference of the superconductor phase difference of two superconducting reservoirs and the azimuthal angle differences of the magnetization direction of the two ferromagnetic spacer layers in the SHS junction. In the framework of the scattering matrix approach, this observation follows directly from the fact that the phase of the superconductor and the azimuthal angle of the ferromagnetic spacer at an HS interface enter in identical ways in the calculation of the Andreev reflection amplitude. Further symmetry considerations showed that the supercurrent is an odd function of the variable $\tilde{\phi}$. Similarly to earlier works,[10,11,14,15] we also find that for symmetric ferromagnetic spacers, $\psi=\psi'$, $\rho=\rho'$, and $\theta=\theta'$, the sign of the current is the opposite to the case of conventional SNS junctions (see Figs. 6, 7, and 9). Consequently, the equilibrium phase difference corresponds to $\phi-\phi'=\pi$, i.e., a π-junction behavior is realized. For independent configurations in F and F′, the equilibrium phase difference varies continuously as the function of interface parameters.

It is worthwhile to compare our results for the Josephson current in single-channel SHS systems to the result for single-channel SNS systems. In the latter case, at zero temperature and in the absence of magnetic field, for a perfectly transparent normal region, the (per spin) Josephson current is given by[24] $I=(e\Delta/2\hbar)\sin(\phi/2)$ for short junctions and[25] $I=ev_F\phi/2\pi L$ for long junctions, where $|\phi|<\pi$. We found [see Eqs. (39) and (35)] that in the case of single-channel SHS systems, in the special point $\sin^2\theta=\sin^2\theta'=\sin^2\rho=\sin^2\rho'=1$, the current-phase relation is identical apart from the phase shifts due to the azimuthal angles and s. Away from the special point, the current-phase relation becomes sinusoidal similar (apart from the phase shifts) to the case of a normal region with low transparency. By adjusting the interface parameters, the single-mode triplet Josephson current interpolates between the result for the conventional Josephson current through an ideal single-mode channel and through a tunnel barrier. The key property that distinguishes the current phase relation in the triplet Josephson effect through single-mode structures from the conventional Josephson effect is the magnetization-dependent phase shift. This is a feature that is common between the fully quantum-mechanical single-channel limit and the multimode case corresponding to the quasiclassics.

We end by relating our results about HS junctions to a possible experiment. One experimental setup could be the HS quantum point contact sketched in Fig. 3. Such a setup is somewhat subtle, as it relies on the presence of a surface magnetization in the point contact. The generality of our proof in the Appendix suggests, however, that the main features of the single-channel HS conductance, i.e., $G=0$ at Fermi level and $G\neq 0$ for $0<eV<\Delta$ could be tested in an experimentally more robust arrangement. Such a setup could be a single-channel point contact to an FS junction, as sketched in Fig. 10. It is not necessary to have the system in the short junction limit, and there can be arbitrary number of modes at the ferromagnet-superconducting interface. The only important detail is that the junction ends in a single-mode point contact through which only one spin direction can be transmitted. This can be achieved using a half-metallic electrode or with a spin filtering quantum point contact.[26]

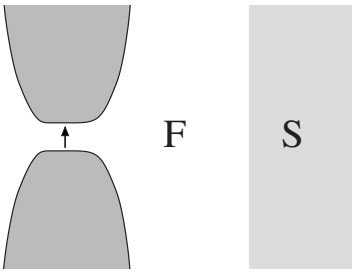

FIG. 10. Sketch of a possible experimental setup for testing the vanishing Andreev reflection at the Fermi level: a single-channel quantum point contact to an FS junction. The arrow in the quantum point contact indicates that the point contact transmits only one spin direction.

ACKNOWLEDGMENTS

We thank A. R. Akhmerov, H. Schomerus, and I. Snyman for valuable discussions. This work was supported by the Dutch Science Foundation NWO/FOM, the Cornell Center for Materials research under NSF Grant No. DMR 0520404, the Packard Foundation, and by the NSF under Grant No. DMR 0705476.

APPENDIX: ABSENCE OF ANDREEV REFLECTION FOR SINGLE-MODE HS JUNCTIONS

In this appendix we prove that, generically, the Andreev reflection amplitude $r_{he}(0)=0$ for a junction with $N=1$ orbital modes in the half-metallic side. The number of modes on the superconducting side can be arbitrary. The starting point of the proof is the singular-value decomposition of the scattering matrix S of the nonsuperconducting region between the half-metallic and superconducting reservoirs,[18]

$$S=\begin{pmatrix} V & 0 \\ 0 & W \end{pmatrix}\begin{pmatrix} \hat{R} & \hat{T}^T \\ \hat{T} & -R' \end{pmatrix}\begin{pmatrix} V' & 0 \\ 0 & W' \end{pmatrix}. \tag{A1}$$

Here, V and V' are $N\times N$ unitary matrices, W and W' are unitary matrices of dimension $2N_S$, with N_S being the number of orbital channels at the normal-metal–superconductor interface, $\hat{T}$ is an $2N_S\times N$ matrix with

$$\hat{T}_{kl}=\delta_{kl}\sqrt{\tau_l},\quad k=1,\ldots,2N_S,\quad l=1,\ldots,N, \tag{A2}$$

with τ_l the lth transmission eigenvalue, $l=1,\ldots,N$, and

$$\hat{R}=\sqrt{1_N-\hat{T}^T\hat{T}},\quad \hat{R}'=\sqrt{1_{2N_S}-\hat{T}\hat{T}^T}. \tag{A3}$$

Substituting the decomposition (A1) in Eq. (8), and assuming $\det(1_{2N_S}+r'\sigma_2 r'^{*}\sigma_2)\neq 0$, one finds

$$r_{\mathrm{he}}(0) = -e^{-i\phi}V^{*}\hat{T}^{T}(Z^{\dagger} - \hat{R}'Z^{*}\hat{R}')^{-1}\hat{T}V' \tag{A4}$$

with $Z=W'^{*}\sigma_2 W$. If $N=1$, the amplitude $r_{\mathrm{he}}(0)$ is proportional to the 11 elements of the inverse in Eq. (A4). Using the general result $A^{-1}=(\det A)^{-1}\mathrm{adj}(A)$ for the matrix inverse, we find that this element is proportional to the determinant of an antisymmetric matrix of dimension $2N_S-1$ and is therefore zero. The case $r_{\mathrm{he}}(0)\neq 0$ is possible if $\det(\mathbb{1}_{2N_S}+r'\sigma_2 r'^{*}\sigma_2)=0$, that is, if the system has an Andreev bound state at $\varepsilon=0$ that is not coupled to the mode in the half-metal. For the ballistic HS system in Sec. III B,

$$\det(\mathbb{1}_{2N_S}+r'\sigma_2 r'^{*}\sigma_2) = 1-\sin^2\rho\,\sin^2\theta, \tag{A5}$$

resulting in $\sin^2\rho=\sin^2\theta=1$ to be the only points where $r_{\mathrm{he}}(0)$ can be nonzero.

[1] R. S. Keizer, S. T. Goennenwein, T. M. Klapwijk, G. Miao, G. Xiao, and A. Gupta, Nature (London) **439**, 825 (2006).
[2] R. A. de Groot, F. M. Mueller, P. G. van Engen, and K. H. J. Buschow, Phys. Rev. Lett. **50**, 2024 (1983).
[3] W. Pickett and J. Moodera, Phys. Today **54** (5), 39 (2001).
[4] J. Coey and M. Venkatesan, J. Appl. Phys. **91**, 8345 (2002).
[5] F. S. Bergeret, A. F. Volkov, and K. B. Efetov, Phys. Rev. Lett. **86**, 4096 (2001a).
[6] A. Kadigrobov, R. I. Shekhter, and M. Jonson, Europhys. Lett. **54**, 394 (2001).
[7] F. S. Bergeret, A. F. Volkov, and K. B. Efetov, Phys. Rev. B **64**, 134506 (2001b).
[8] M. Eschrig, J. Kopu, J. C. Cuevas, and G. Schon, Phys. Rev. Lett. **90**, 137003 (2003).
[9] F. S. Bergeret, A. F. Volkov, and K. B. Efetov, Rev. Mod. Phys. **77**, 1321 (2005).
[10] V. Braude and Y. V. Nazarov, Phys. Rev. Lett. **98**, 077003 (2007).
[11] M. Eschrig, T. Löfwander, T. Champel, J. Cuevas, J. Kopu, and G. Schön, J. Low Temp. Phys. **147**, 457 (2007).
[12] Y. Asano, Y. Tanaka, and A. A. Golubov, Phys. Rev. Lett. **98**, 107002 (2007).
[13] Y. Asano, Y. Sawa, Y. Tanaka, and A. A. Golubov, Phys. Rev. B **76**, 224525 (2007).
[14] M. Eschrig and T. Löfwander, Nat. Phys. **4**, 138 (2008).
[15] A. V. Galaktionov, M. S. Kalenkov, and A. D. Zaikin, Phys. Rev. B **77**, 094520 (2008).
[16] G. Eilenberger, Z. Phys. **214**, 195 (1968).
[17] A. I. Larkin and Y. N. Ovchinnikov, Sov. Phys. JETP **28**, 1200 (1969).
[18] C. W. J. Beenakker, Rev. Mod. Phys. **69**, 731 (1997).
[19] J. Yi-Qun, N. Zhi-Ping, F. Cui-Di, and X. Ding-Yu, Chin. Phys. Lett. **25**, 691 (2008).
[20] G. E. Blonder, M. Tinkham, and T. M. Klapwijk, Phys. Rev. B **25**, 4515 (1982).
[21] Y. Takane and H. Ebisawa, J. Phys. Soc. Jpn. **61**, 1685 (1992).
[22] P. W. Brouwer and C. W. J. Beenakker, Chaos, Solitons Fractals **8**, 1249 (1997).
[23] C. W. J. Beenakker, Phys. Rev. B **46**, 12841 (1992).
[24] C. W. J. Beenakker, in *Transport Phenomena in Mesoscopic Systems*, edited by H. Fukuyama and T. Ando (Springer, Berlin, 1992), p. 235.
[25] C. Ishii, Prog. Theor. Phys. **44**, 1525 (1970).
[26] R. M. Potok, J. A. Folk, C. M. Marcus, and V. Umansky, Phys. Rev. Lett. **89**, 266602 (2002).